Published in "The Journal of Chemical Physics 144(2): 024301, 2016"
which should be cited to refer to this work.

Resonance effects in elastic cross sections for electron scattering on pyrimidine: Experiment and theory

Khrystyna Regeta,[1] Michael Allan,[1] Carl Winstead,[2] Vincent McKoy,[2] Zdeněk Mašín,[3] and Jimena D. Gorfinkiel[4]
[1]*Department of Chemistry, University of Fribourg, Chemin du Musée 9, CH-1700 Fribourg, Switzerland*
[2]*A. A. Noyes Laboratory of Chemical Physics, California Institute of Technology, Pasadena, California 91125, USA*
[3]*Max-Born Institute for Nonlinear Optics and Short Pulse Spectroscopy, Max-Born-Strasse 2A, 12489 Berlin, Germany*
[4]*Department of Physical Sciences, The Open University, Walton Hall, Milton Keynes MK7 6AA, United Kingdom*

We measured differential cross sections for elastic (rotationally integrated) electron scattering on pyrimidine, both as a function of angle up to 180° at electron energies of 1, 5, 10, and 20 eV and as a function of electron energy in the range 0.1–14 eV. The experimental results are compared to the results of the fixed-nuclei Schwinger variational and R-matrix theoretical methods, which reproduce satisfactorily the magnitudes and shapes of the experimental cross sections. The emphasis of the present work is on recording detailed excitation functions revealing resonances in the excitation process. Resonant structures are observed at 0.2, 0.7, and 4.35 eV and calculations for different symmetries confirm their assignment as the $\tilde{X}^2A_2$, $\tilde{A}^2B_1$, and $\tilde{B}^2B_1$ shape resonances. As a consequence of superposition of coherent resonant amplitudes with background scattering the $\tilde{B}^2B_1$ shape resonance appears as a peak, a dip, or a step function in the cross sections recorded as a function of energy at different scattering angles and this effect is satisfactorily reproduced by theory. The dip and peak contributions at different scattering angles partially compensate, making the resonance nearly invisible in the integral cross section. Vibrationally integrated cross sections were also measured at 1, 5, 10 and 20 eV and the question of whether the fixed-nuclei cross sections should be compared to vibrationally elastic or vibrationally integrated cross section is discussed.

I. INTRODUCTION

Pyrimidine (1,3-diazine, see Fig. 1) is a prototype aromatic heterocyclic compound. It serves as a simple model compound for the nucleobases cytosine, thymine, and uracil, making electron collisions with pyrimidine relevant for radiation damage to living tissue and thus for cancer radiotherapy.[1]

Experimental elastic cross sections for pyrimidine, accompanied by the *ab initio* Schwinger multichannel variational (SMC) and by the screened additivity rule method (IAM-SCAR) calculations, were presented by Palihawadana *et al.*[2] They measured differential cross sections (DCSs) for elastic scattering at angles in the range 10°-129° and the energy range from 3 to 50 eV, and integrated them to obtain the integral cross sections (ICSs). A theoretical study of elastic scattering from pyrimidine using the R-matrix method, accompanied by experimental and theoretical studies of electronic excitation, was performed by Mašín *et al.*[3] Elastic differential, integral, and momentum-transfer cross sections, as well as total (elastic + inelastic) and total absorption cross sections for impact energies ranging from 0.2 to 500 eV were calculated by Ferraz *et al.* using a technique involving numerical solution of the Lippmann-Schwinger equation for a potential that included an absorbing term, obtained from the semiempirical scaled quasifree-scattering-model (SQFSM), to account for the effect of inelastic scattering channels.[4] A recent theoretical study combining several theoretical methods—the single-centre expansion (ePOLYSCAT), the R-matrix method, and a corrected form of the independent-atom representation (IAM-SCAR)— to cover a wide energy range was reported by Sanz *et al.*[5] Experimental DCSs for elastic scattering of electrons from pyrimidine at higher electron energies (50-300 eV) were reported by Maljković *et al.*[6] Related to the present study are the measurements of the total cross sections by Fuss *et al.*[7] and Baek *et al.*[8] The energies of shape resonances in pyrimidine, which affect the elastic cross sections, were studied by electron transmission spectroscopy (ETS) by Nenner and Schulz[9] and by Modelli *et al.*[10] The experimentally and theoretically determined cross sections were paramount for charged-particle track simulations employed by Fuss *et al.* to quantify the induced physicochemical and potential biological implications when primary ionizing particles strike a medium made up of pyrimidine.[11]

The present work aims at extending the existing studies to larger scattering angles and lower energies. We emphasize the details of the excitation functions, i.e., the DCSs plotted as a function of electron energy, which reveal the role of resonances. We present the rotationally integrated and

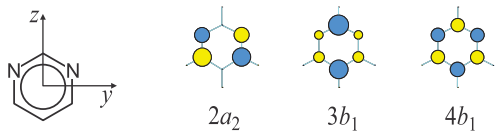

FIG. 1. Structure of pyrimidine and schematic representations of virtual orbitals whose temporary occupation gives rise to shape resonances.

vibrationally elastic, but also both the rotationally and vibrationally integrated cross sections. Data in numerical form are given in the supplementary material.[12]

II. ELECTRON IMPACT SPECTROMETER

The spectrometer and the procedures used to measure the absolute cross sections are the same as in our recent work on furan.[13] The measurements were performed using an electron-impact spectrometer described earlier.[14,15] It employs hemispherical analyzers to improve resolution, which was set to 24 meV (in the energy-loss mode) for the present study, and with a magnetic angle changer[16,17] to access scattering angles up to 180°. The electron beam current was 300-700 pA. The energy of the incident electrons was calibrated on the 19.365 eV ^{2}S resonance in helium[18] and is accurate to within ±10 meV. The sensitivity of the instrument is not constant when the electron energies are varied, but this effect, expressed as the "instrumental response function," was quantified on elastic scattering in helium and all spectra were corrected as described earlier.[14,15] The values of the cross sections were determined by the relative flow technique as described by Nickel *et al.*[19] using the theoretical helium elastic cross sections of Nesbet[20] as a reference. The vibrationally inelastic cross sections were then determined by comparing the areas under the elastic peak, integrated in the energy-loss range from −0.035 eV to +0.035 eV, and the vibrational excitation bands, integrated in the energy-loss range from 0.035 eV to 1.2 eV. The confidence limit of the magnitudes of the elastic cross sections is ±15%. The pyrimidine and helium pressures in the gas inlet line were typically 0.08 and 0.24 mbar, respectively, during the absolute measurements.

III. THEORETICAL APPROACHES

A. Schwinger multichannel method

We used the Schwinger multichannel (SMC) procedure[21,22] as implemented for parallel computers.[23,24] All details of the present calculation on pyrimidine are as described in Ref. 2.

B. R-matrix method: Theory and characteristics of the calculation

A detailed description of the R-matrix method and its application to electron-molecule scattering can be found elsewhere[25,26] so we will not repeat it here. The calculations reported in this work have been performed with the UKRmol+ suite, a re-engineered version of the UKRmol codes.[27] This new parallel suite is capable of determining the molecular integrals in quadruple precision, enabling an improved description of the scattering electron. POLYDCS[28] has been used to determine the DCSs. The R-matrix results presented here correspond to the use of the cc-pVDZ basis set and the close-coupling scattering model, including 29 electronic states (further details can be found in Ref. 29). However, they differ slightly from those published earlier: the new suite has allowed us to use in the calculation the complete set of molecular continuum functions generated by the same continuum atomic basis set. In practice, this corresponded to using deletion thresholds of 10^{-14} instead of 10^{-7} as in our previous work.[29] There are no significant changes to the cross sections as a result of the improvement of the continuum, thus confirming the quality of earlier results.

IV. RESULTS

A. Angular distributions

The present angular distributions of the cross sections are compared to published experimental data in Fig. 2 and to the SMC and R-matrix calculated data in Figs. 3 and 4.

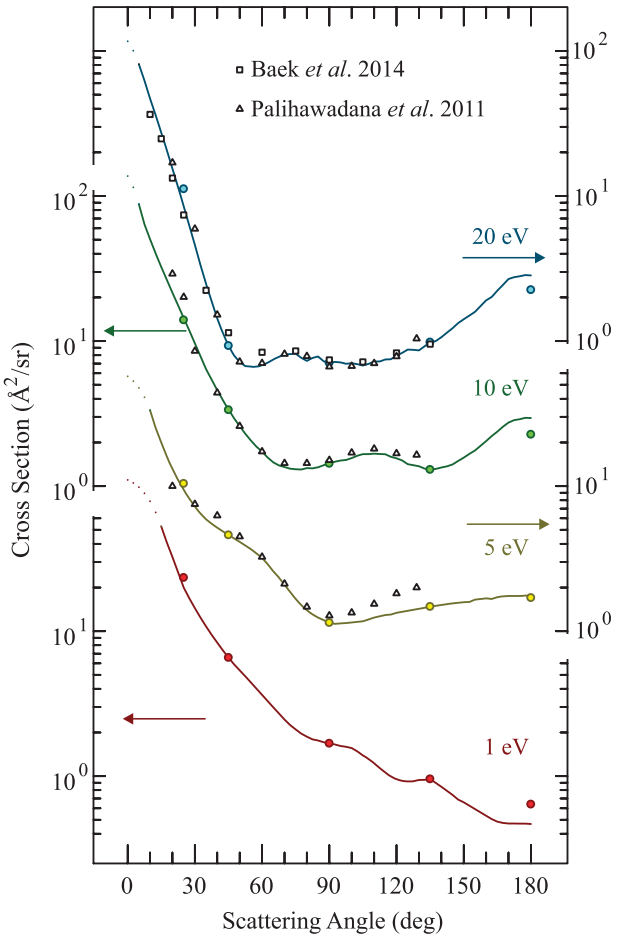

FIG. 2. Angular distributions of the elastic DCS. Continuous lines and circles show the present data. Squares show the experimental data of Baek *et al.*,[30] triangles that of Palihawadana *et al.*[2] (their 6 eV data is compared to our 5 eV data). The top 3 spectra are shown offset by a factor of 10 each. The horizontal arrows point to the appropriate ordinate scales. Colored dots show how the experimental data were visually extrapolated down to 0° to obtain the integral cross sections.

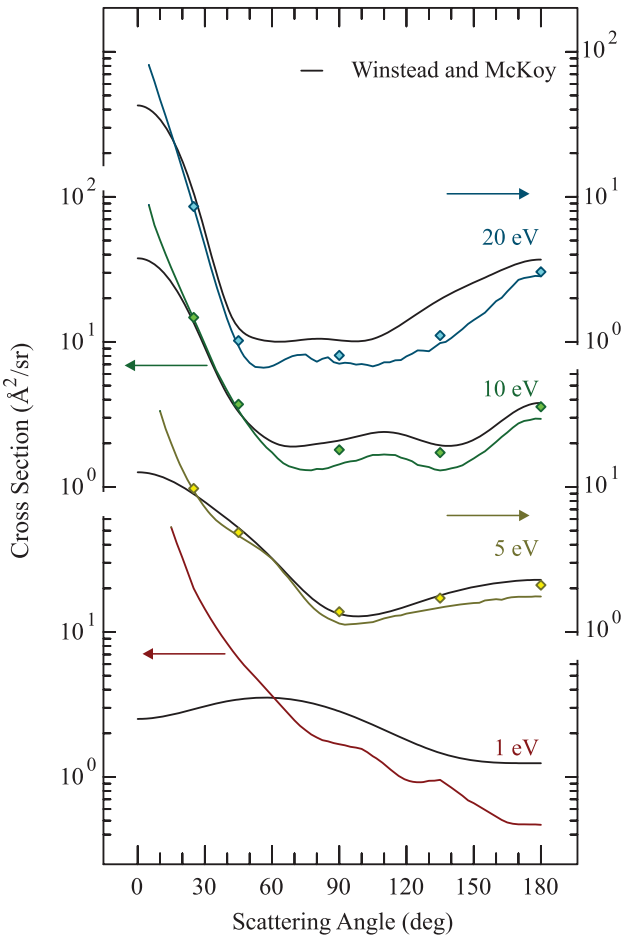

FIG. 3. Comparison of the present experimental DCS (colored lines) with the calculated results of Winstead and McKoy (Ref. 2 and this work) (black lines). Diamonds indicate sums of elastic and vibrationally inelastic (all modes) cross sections.

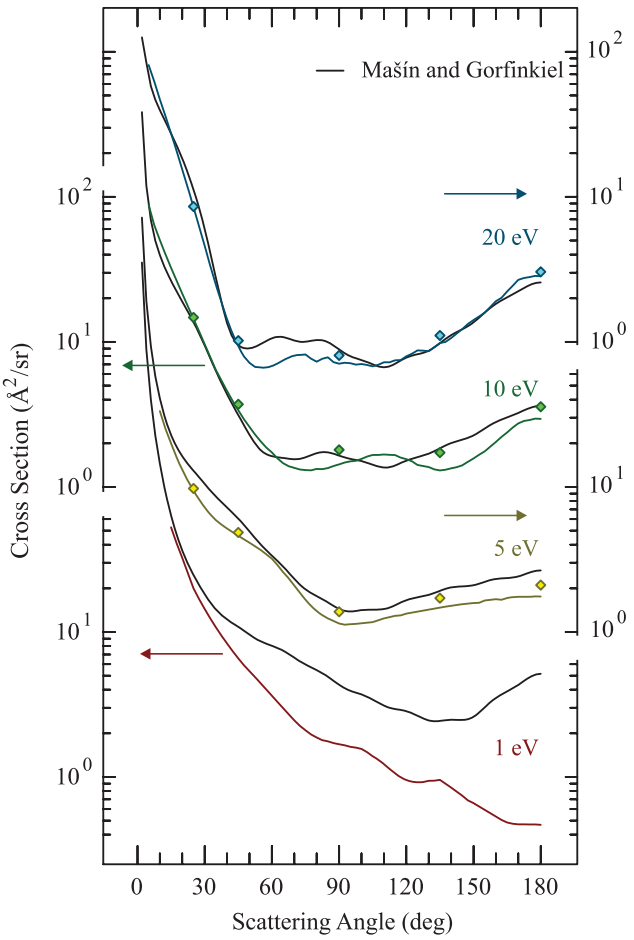

FIG. 4. Comparison of the present experimental DCS (colored lines) with the calculated results of Mašín and Gorfinkiel (Ref. 3 and this work) (black lines). Diamonds indicate sums of elastic and vibrationally inelastic (all modes) cross sections.

The present experimental data were obtained in two steps. First absolute values of the elastic cross section were determined by the relative flow method at the scattering angles of 25°, 45°, 90°, 135°, and 180° and these values are shown in Fig. 2 as circles. The detailed shapes of the cross section as a function of angle were then obtained by scanning the magnetic angle changer, in steps of 2.5°, around the fixed analyzer positions of 25°, 45°, 90°, and 135° and then combining the four segments into one curve, which was normalized to the discrete absolute values. These data are shown by colored continuous lines in Figs. 2-4. The fact that 5 independent absolute values at various angles were measured instead of only one provides a consistency check of the procedure. Our data compare favorably with the earlier experimental results shown in Fig. 2—the agreement with both the data of Baek *et al.*[30] and Palihawadana *et al.*[2] is excellent.

Fig. 3 compares the present experimental data with the cross section computed using the SMC variational procedure as already reported in Ref. 2 but expanded for the purpose of the present work. There is an excellent agreement in the shapes of the curves at 5, 10, and 20 eV, including in the region 135°-180° made accessible by the magnetic angle changer. At low scattering angles, the experimental cross section rises steeply because of long-range scattering by the dipole field caused by the dipole moment of pyrimidine (2.3 D, see Ref. 31) and this effect is not included in the SMC calculations. The effect is strongest in the 1 eV spectrum. Apart from this effect the agreement of the absolute values is satisfactory although the measured values are lower in the 60°–180° range, in particular, at 10 eV and 20 eV.

A Born correction for scattering by the long range dipole field has been applied to the R-matrix data in Fig. 4 via the use of POLYDCS; the correction is based on inclusion of rotational motion and is thus dependent on the initial and final rotational states. Technical limitations allow us to compute rotationally summed cross sections only for molecules initially in the rotational ground state. At nonzero temperatures, higher rotational levels are populated, average rotational energy losses are larger, and the dipolar contribution to the cross section is decreased. Franz and Gianturco recently argued[32] that temperature effects on the dipole-corrected ICS for positron scattering by pyrimidine are negligible, which would imply that such effects should also be negligible in electron scattering. However, Okamoto *et al.*[33] previously demonstrated a temperature effect in the ICS for elastic electron-water scattering, with the 0 K and 300 K cross sections differing by 9% at 6 eV. Temperature effects will be larger in heavier molecules such as pyrimidine, where much

higher rotational levels are populated at room temperature. As a result, we expect our rotationally summed ICS to be significantly larger than the ICS that would be measured in room-temperature experiments. As discussed by Okamoto *et al.*,[33] this temperature effect arises from scattering at extreme forward angles and so does not affect the DCS comparisons shown in Fig. 4.

The agreement with experiment is very good down to the lowest experimentally accessible angles, which are 5° at 10 and 20 eV, 10° at 5 eV, and 15° at 1 eV. Very good agreement is found also in the intermediate and high angular range. For both theoretical models, the agreement becomes worse at the low energy of 1 eV.

Ab initio models which include only the elastic scattering channel and therefore neglect inelastic open channels (electronic excitation and ionization) tend to overestimate the cross sections at higher energies and intermediate and high scattering angles. Inclusion of these channels leads to a reduction of the electronic flux in the elastic scattering channel and therefore the cross section. The R-matrix calculations in this work include electronically excited states up to 10.51 eV (but no ionization channels). The better agreement of the R-matrix DCS at higher energies (in size if not shape at 10 eV) can be ascribed to this inclusion.

One may ask whether the exclusion of the vibrationally inelastic processes in the experimental data may not also contribute to the difference. In other words, should cross sections calculated in the fixed-nuclei approximation be compared to the vibrationally elastic or vibrationally integrated experimental cross section? To show how large the difference is, we measured the vibrationally integrated cross section by integrating under not only the elastic peak, but also under all vibrationally inelastic peaks up to an energy loss of 1.2 eV and indicate the results as diamonds in Figs. 3 and 4. We note that the inclusion of the vibrationally inelastic channels reduces the difference between theory and experiment, although differences attributable to the neglect of open electronically inelastic channels remain.

The approximation of computing cross sections with the nuclei fixed at the equilibrium geometry is common in calculations and depends on three component approximations: that the collision takes place on a time scale short compared to vibrational motion, that vibrational energy losses are negligible compared to the collision energy, and that the dependence of the scattering amplitude on nuclear coordinates is weak. The first two of these constitute the adiabatic approximation for vibration[34,35] and allow vibrational state-to-state excitation amplitudes $F(v \to v')$ to be computed as matrix elements of the fixed-nuclei elastic scattering amplitude between vibrational states χ_v,

$$F(v \to v') = \int dQ\, \chi_v(Q) f(Q) \chi_{v'}(Q), \tag{1}$$

where Q collectively represents the vibrational coordinates and $f(Q)$ is the fixed-nuclei amplitude at Q. The third allows us to replace $f(Q)$ by its value $f(Q_{\mathrm{eq}})$ at equilibrium and take it outside integrals over nuclear coordinates. If we do so at the outset, we find

$$F(v \to v') \approx f(Q_{\mathrm{eq}}) \int dQ\, \chi_v(Q) \chi_{v'}(Q) = f(Q_{\mathrm{eq}}) \delta_{v,v'}, \tag{2}$$

so only vibrationally elastic scattering is allowed. However, following Lane,[36] we may also use the adiabatic approximation to write the vibrationally summed cross section as

$$\sum_{v'} |F(v \to v')|^2 = \int dQ\, \chi_v(Q) |f(Q)|^2 \chi_v(Q), \tag{3}$$

where we have used completeness to eliminate the sum on v'. If we now approximate $f(Q)$ by $f(Q_{\mathrm{eq}})$, we obtain the result that the fixed-nuclei cross section $|f(Q_{\mathrm{eq}})|^2$ approximates the vibrationally summed cross section without reference to individual state-to-state cross sections. We may summarize the situation by saying that the single-geometry fixed-nuclei elastic cross section may be compared to the vibrationally summed cross section when all three underlying approximations are valid, and that, as a corollary, vibrationally elastic scattering will be the dominant contribution to the sum in such cases. The results shown in Figs. 3 and 4 appear to reflect these conditions being well satisfied in pyrimidine at 5 eV and above.

The present data also agree well with the calculated cross sections of Ferraz *et al.*[4] Their results agree nearly perfectly with the experiment of Palihawadana *et al.*[2] at 10 eV and thus necessarily with our data which are nearly identical (Fig. 2). Their results are also slightly higher than the experiment at 20 eV in the intermediate angular range.

B. Integral cross sections

Determination of experimental integral cross sections by integrating the differential cross sections in Fig. 2 is hampered by the large dipole moment of pyrimidine and the ensuing long range scattering. The fixed-nuclei elastic differential cross section for a polar molecule is infinite at 0°, the partial-wave series for the corresponding scattering amplitude does not converge, and the associated integral cross section is infinite. Fixed-nuclei calculations typically cover only a finite number of partial waves (as in the R-matrix work) or a finite region of space (as in the SMC work). For that reason, the calculated results do not reflect these divergences, but at the same time they need to be corrected, or topped up, for the effect of long-range (or equivalently high partial wave) scattering from the dipole potential. The corrections attain large values—as an example the Born correction as applied here in connection with the R-matrix theory yields a 0° cross section of 2.5×10^{12} Å^2, which makes it dominate the integral cross section despite the solid angle factor $\sin(\theta)$ which becomes zero at 0°.[3,37]

This cross section cannot be measured—the instrument has an (energy-dependent) angular resolution which is about 6° (full angle) at 10 eV so that at an analyser setting below 3°, the instrument cannot distinguish between unscattered and elastically scattered electrons. Apart from this there is probably no situation where elastic scattering at much below 1° correctly describes reality: in reality the very large impact parameters become comparable to the diameter of the electron

beam, at large impact parameters the electron interacts with several molecules simultaneously because of finite target gas density and electrons are deflected to small angles by other weak fields caused by nearby objects.

To summarize, it is unfortunate but true that a significant contribution to the ICS of a polar molecule comes from an angular range where measurements are very difficult and where the validity of approximations underlying the calculations is questionable but not subject to an easy test.

One strategy for comparing theory and experiment would be to integrate both experiment and theory only in the experimentally accessible range, i.e., 5°-180° at 10 and 20 eV. The disadvantage is that this procedure introduces an arbitrary parameter and leaves the problem of obtaining a universal ("true") ICS unresolved. Moreover, the comparison of differential cross sections in Figs. 3 and 4 yields a more detailed and precise information than a comparison of cross sections integrated over an incomplete angular range.

Despite the fundamental problems listed above, a pragmatic "integral cross section," excluding the diverging part below 2°, appears to be a useful quantity which we obtain by integrating under differential cross sections visually extrapolated down to 0° as shown in Fig. 2. The detailed shape of the extrapolated section, as long as it does not rise to exotically large values, affects the integral cross section only weakly because of the $\sin(\theta)$ weighting factor in the integration. The results are given in Table I. The agreement with the experimental data of Palihawadana *et al.*[2] is very good. Our 1 eV data point in Table I indicates a steep rise of the ICS at low energies. The present R-matrix results excluding the Born correction also agree very well with both experiments, including at low energies. (The energies of 1 eV and 5 eV lie within the range of the calculated shape resonances, which are too narrow and consequently too large in magnitude because of the neglect of nuclear motion, making the calculated cross sections at these energies too large. The agreement with experiment is even better if this effect is taken into account.)

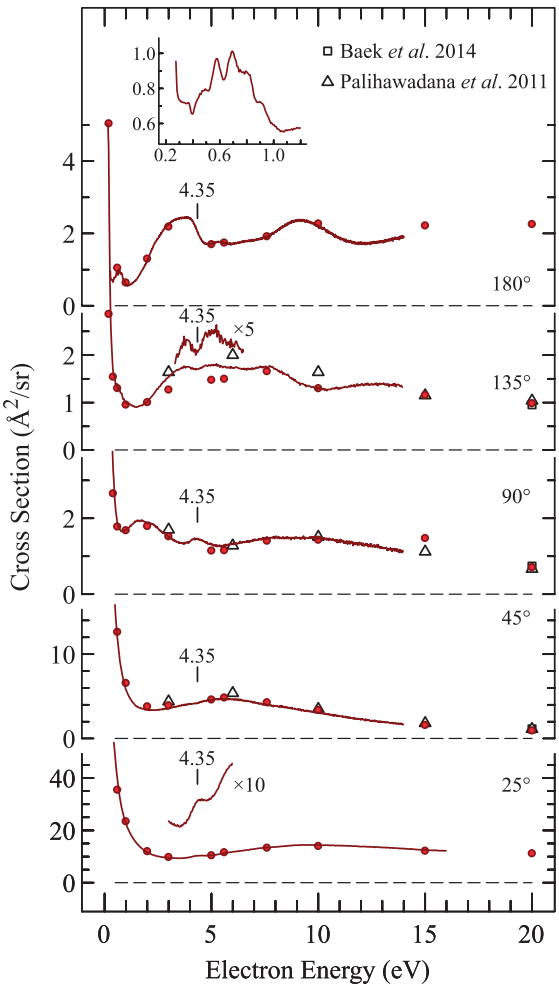

FIG. 5. Elastic differential cross sections plotted as a function of incident electron energy. Continuous lines and circles show the present data. Squares show the experimental data of Baek *et al.*[30] triangles that of Palihawadana *et al.*[2] (average of their 40° and 50° data is compared to our 45° data, their 129° data to our 135° data). The position of the 4.35 eV shape resonance is marked. The inset shows a low energy detail of the 180° spectrum with vibrational structure.

C. Dependence on electron energy

The elastic cross sections were recorded as a function of electron energy and the results are compared with published experiments in Fig. 5 and with the SMC and R-matrix calculations in Figs. 6 and 7. Similarly to the angular distributions, the measurements were performed in two steps. Absolute cross sections were first determined by the relative flow method at 10-13 different energies and the results are indicated by red circles in Fig. 5. Excitation functions were then recorded, corrected for the response function, and normalized to the absolute measurements. The redundancy given by the large number of absolute measurements provides a check of consistency of the data. The agreement with the earlier experimental data of Baek *et al.*[30] and of Palihawadana *et al.*[2] shown for comparison in Fig. 5 is excellent. In some cases it may even be difficult to distinguish the symbols—at 45°, 90°, and 135° and 20 eV the circle, triangle, and square nearly coincide.

Fig. 6 compares the experimental spectra with the SMC results of Winstead and McKoy (Ref. 2 and this work). There is generally a good agreement in the magnitude of the cross section. The exceptions are the larger calculated cross section at 180° and above 10 eV, and the low calculated cross section at 25° and below 3 eV. Fig. 7 compares the experimental spectra with the R-matrix results. Again, the agreement is generally good, with the calculated cross section being again too large for 180°. The improved agreement with experiment for 25° is due to the use of the Born correction.

TABLE I. Integral elastic cross sections, in Å^2. Given is the present experimental data (±20%), the experimental data of Ref. 2 and the R-matrix and the SMC data, both without Born correction.

Energy (eV)	1	3	5	6	10	15	20
Experiment	62.7	...	39.0	...	45.9	...	29.8
Expt. Ref. 2	...	37.5	...	35.0	45.0	37.1	35.9
R-matrix	74.8	40.9	41.2	36.0	39.4	36.7	28.5
SMC	32.2	31.2	36.4	36.3	45.6	43.0	33.3

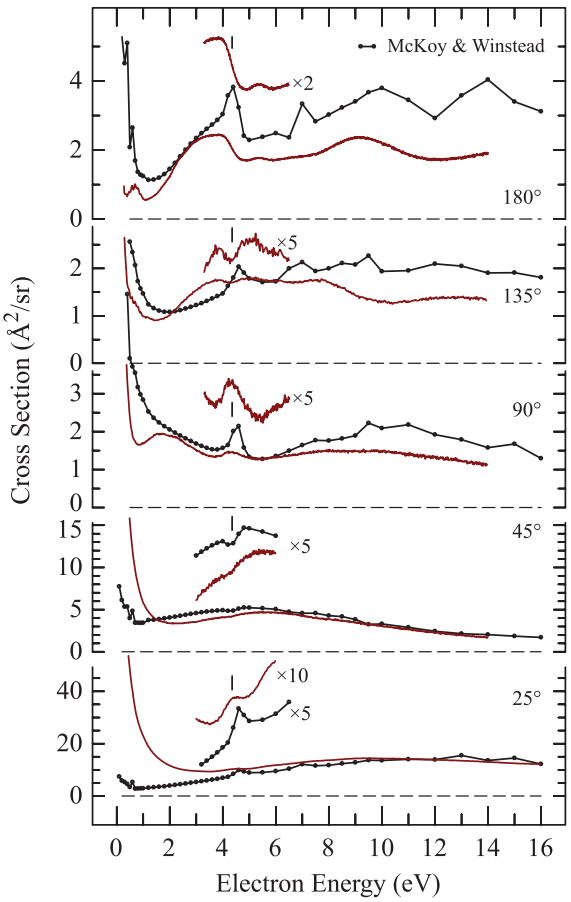

FIG. 6. Comparison of the experimental DCS with the calculated results of Winstead and McKoy (Ref. 2 and this work). The position of the 4.35 eV shape resonance is marked.

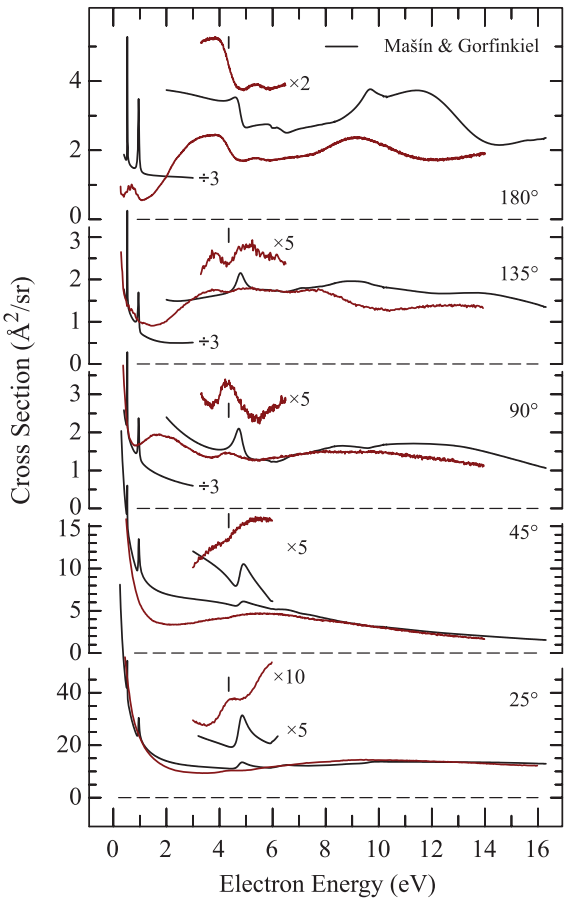

FIG. 7. Comparison of the experimental DCS with the calculated results of Mašín and Gorfinkiel (Ref. 3 and this work) (black lines). The position of the 4.35 eV shape resonance is marked.

The three well known shape resonances cause structures on the experimental cross section. The lowest, $\tilde{X}\,^2A_2$, is superimposed on the steep rise of the cross section at low energies and can be discerned only on the derivative of the 135° DCS (not shown), at 0.2 eV. It is uncertain whether this corresponds to the vertical attachment energy because the ground vibrational level of this anionic state may be bound and thus not visible.[9] The next resonance, $\tilde{A}\,^2B_1$, is visible as structures on the 180° and 135° spectra, centered (i.e., vertical attachment energy) at 0.7 eV. The third shape resonance, $\tilde{B}\,^2B_1$, is centered at 4.35 eV. These values are in satisfactory agreement with the ETS values of Nenner and Schulz,[9] 0.25, 0.77, and 4.24 eV, and of Modelli *et al.*[10] 0.39, 0.82, and 4.26 eV. Small differences, in particular for the two lower resonances, are not due to energy scale calibration problems, but to the fact that different techniques (ETS, elastic CS at different angles, CS for vibrational excitations) enhance different vibrational (boomerang) features to different degrees, so that the observed center of the band depends on the technique used.

There is a very good agreement between experiment and theory in the positions of the resonances. The width of the resonant structures in the fixed-nuclei calculated cross sections is given only by the electronic width Γ and is thus narrower than the experimental width of the band which is augmented because a whole range of nuclear coordinates is probed, that is, by the width of the Franck-Condon profile of the band. The broad Franck-Condon profiles consist of progressions of narrow vibrational (boomerang) peaks for the two low-lying shape resonances $\tilde{X}\,^2A_2$ and $\tilde{A}\,^2B_1$ (the latter is shown enlarged as an insert in Fig. 5), indicating that the electronic widths of these two resonances are comparable to, or narrower than, the vibrational spacing. The experiment thus confirms the narrow calculated electronic widths of these two resonances. Similarly the absence of vibrational structure on the third resonance $\tilde{B}\,^2B_1$ confirms the calculated width being wider than vibrational spacing. The calculations correctly reproduce that the A^2B_1 shape resonance is best visible in the 180° spectrum.

Interesting is the shape of the $\tilde{B}\,^2B_1$ resonance structure around 4.35 eV. It appears as a peak at 25° and 90°, and as a dip at 45° and these shapes are qualitatively correctly reproduced by theory (except for the dip at 45° that is more of a step in the R-matrix calculations). Both theory results also correctly reproduce the step-down shape in the 180° spectrum. Disagreement appears at 135°, where experiment shows a dip shape whereas theory indicates a peak. These dip and peak shapes can be traced back, analyzing the contributions of the calculated scattering amplitudes for the partial wave channels, to coherent superposition of the background and resonant contributions to the *p*-wave elastic scattering amplitude. The varying peak- and dip-shapes have the consequence that the

resonant structure is very shallow in the integral cross section as shown below.

A weaker peak is observed at 5.35 eV, in particular in the 180° spectrum (magnified view in the top traces in Figs. 6 and 7). It has been reported in ETS by Modelli *et al.*[10] and assigned as a core excited resonance. It is pronounced in cross sections for electronic excitation and will be discussed in the accompanying paper.[38]

The shapes of the experimental cross sections as a function of energy from Fig. 5 were summed, with appropriate weights, as described in Ref. 15, to obtain the integral cross section as a function of energy shown in Fig. 8. The result is only approximate in the sense that spectra recorded at only 5 angles were summed and that the diverging behavior of the cross section near 0° is ignored. An indication of the magnitude of the first contribution to the error is given by the agreement with the more reliable ICS values from Table I, shown as red circles in Fig. 8, obtained from angular data with a much finer (2.5°) spacing.

The ICSs are compared to the theoretical work of Mašín, Gorfinkiel and coworkers (Refs. 3, 37 and this work) in Fig. 8 (the Born corrected cross sections can be seen in Refs. 3 and 29). There is a very good agreement in the absolute magnitude of the cross section and in the fact that the cross section rises steeply at low energies. The agreement of the shapes is satisfactory when the approximate nature of the experimental curve is taken into account. The two low-lying resonances appear very high and narrow in the calculation — a natural consequence of the fixed-nuclei approximation as already discussed above. The experimental peaks are much broader, correspondingly shallower, and nearly disappear under the fast rising background. The 4.35 eV resonance also appears broader and shallower in the experiment than in theory. Its contribution to the ICS is much weaker than to the DCSs in Fig. 6 because of compensation of peak and dip shapes

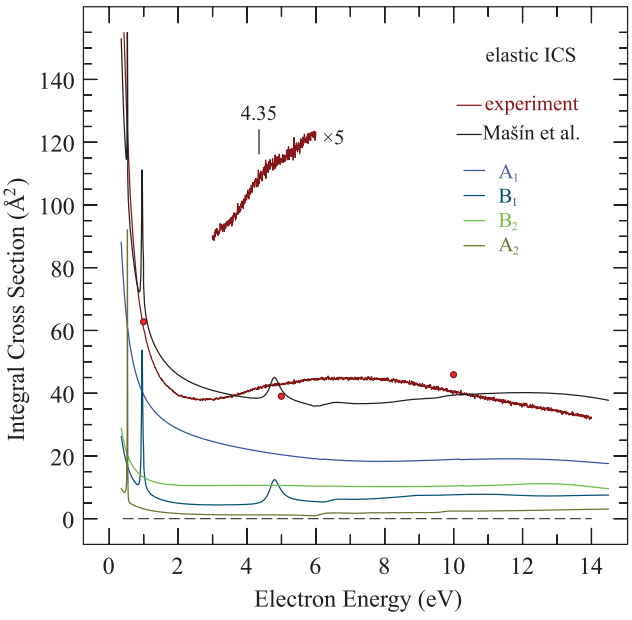

FIG. 8. Comparison of the experimental ICS with the calculated results (without Born correction) of Mašín *et al.* (Ref. 3 and this work). The contributions of all symmetries are indicated.

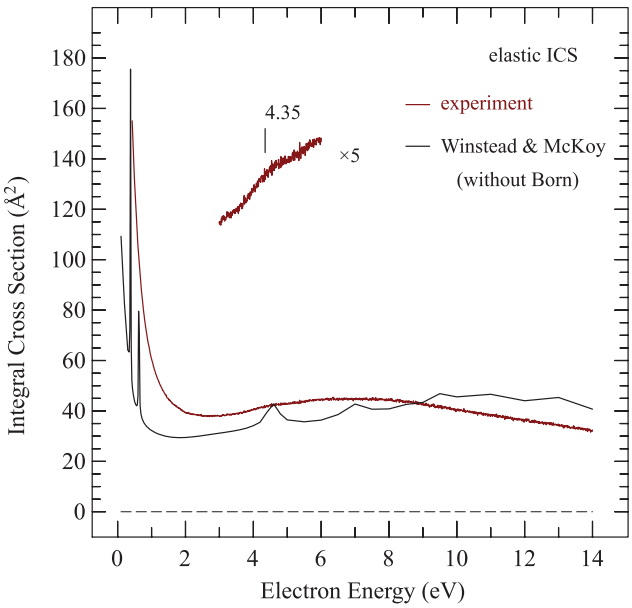

FIG. 9. Comparison of the experimental ICS with the results of Winstead and McKoy (Ref. 2 and this work).

as already discussed above. The contributions of the different symmetries to the ICS, shown in Fig. 8, confirm that the lowest resonance is of A_2 symmetry, the second and third resonances of B_1 symmetry.

The agreement with the SMC calculation of Winstead and McKoy shown in Fig. 9 is as would be expected from Fig. 3. The calculated cross section is slightly below experiment at low energies because the DCS on which it is based starts to decrease already around 10°-15° as seen in Fig. 3. The two low-lying resonances are calculated very narrow and high because of the neglect of boomerang motion which broadens the band in the experiment.

V. CONCLUSIONS

We present a stringent test of the capacity of theory to reproduce the details of elastic cross sections in pyrimidine. This is achieved by comparing both differential and integral cross sections by extending the angular range to 180° using the magnetic angle changer and by comparing the detailed shapes of the cross section as a function of electron energy.

Very good agreement was found in many aspects as follows.

- The magnitudes of the differential cross sections are reproduced very well in the experimentally accessible angular range (5°-180° at 10 and 20 eV, 10°-180° at 5 eV) when the Born correction for the long range scattering by the dipole moment of pyrimidine is taken into account. Theory without Born correction reproduces the measured DCS well for angles above about 15° but expectedly fails to reproduce the steep rise at forward angles.
- The differential cross sections calculated using elastic scattering models are slightly higher than experiment

at higher energies and intermediate and high scattering angles and the difference is attributed primarily to the neglect of open inelastic channels in the calculations.

- The question whether fixed-nuclei calculations should be compared to vibrationally elastic or vibrationally integrated experimental cross sections is addressed. We note that in this case the agreement with theory is improved when vibrationally integrated experimental cross sections are taken.
- Good agreement is found for the energies and widths of the resonances when it is taken into account that the fixed-nuclei calculations do not reproduce the vibrational (boomerang) fine structure (the Franck-Condon profiles) of the resonances. The resolved vibrational structures on the $\tilde{X}\,^2A_2$ and $\tilde{A}\,^2B_1$ resonances provide experimental evidence for an electronic width Γ being narrower than vibrational spacing, the absence of vibrational structure on the $\tilde{B}\,^2B_1$ resonance indicates Γ wider than vibrational spacing, in agreement with the calculations.
- The calculated contributions of the different symmetries to the integral cross section confirm the assignment of the resonances.
- The shape of the 4.35 eV resonant structure in the differential cross sections is a test of how well the theory treats the coherent superposition of the background and resonant amplitudes. The agreement with both the SMC and R-matrix theory is generally very good, the structure being a peak, a dip, or a step function at various angles in both theory and experiment. A certain exception is encountered at 135° where a dip is observed but a peak is calculated.

Finally, we point out the fundamental problems posed by the permanent dipole moment of pyrimidine, and the ensuing diverging theoretical cross section at 0°, for deriving a universally valid and practically useful integral cross section and for comparison of experiment and theory.

ACKNOWLEDGMENTS

This research is part of Project No. 200020-144367/1 of the Swiss National Science Foundation and of the COST Action No. CM1301 CELINA. This material is based in part upon work by C.W. and V.M. supported by the U.S. Department of Energy, Office of Science, Office of Basic Energy Sciences, Chemical Sciences, Geosciences, and Biosciences Division, under Award No. DE-FG02-97ER14814. C.W. and V.M. also acknowledge use of the Jet Propulsion Laboratory's Supercomputing and Visualization Facility. Initial R-matrix calculations were performed as part of the EPSRC funded UK-RAMP Project. Z.M. and J.D.G. acknowledge the support of the ARCHER eCSE01-013 project and the use of the VULCAN computer cluster at the Max-Born Institute.

[1]B. Boudaiffa, P. Cloutier, D. Hunting, M. A. Huels, and L. Sanche, Science **287**, 1658 (2000).
[2]P. Palihawadana, J. Sullivan, M. Brunger, C. Winstead, V. McKoy, G. Garcia, F. Blanco, and S. Buckman, Phys. Rev. A **84**, 062702 (2011).
[3]Z. Mašín, J. D. Gorfinkiel, D. B. Jones, S. M. Bellm, and M. J. Brunger, J. Chem. Phys. **136**, 144310 (2012).
[4]J. R. Ferraz, A. S. dos Santos, G. L. C. de Souza, A. I. Zanelato, T. R. M. Alves, M.-T. Lee, L. M. Brescansin, R. R. Lucchese, and L. E. Machado, Phys. Rev. A **87**, 032717 (2013).
[5]A. G. Sanz, M. C. Fuss, F. Blanco, Z. Mašín, J. D. Gorfinkiel, F. Carelli, F. Sebastianelli, F. A. Gianturco, and G. García, Appl. Radiat. Isot. **83**, 57–67 (2014).
[6]J. B. Maljković, A. R. Milosavljević, F. Blanco, D. Šević, G. García, and B. P. Marinković, Phys. Rev. A **79**, 052706 (2009).
[7]M. C. Fuss, A. G. Sanz, F. Blanco, J. C. Oller, P. Limão-Vieira, M. J. Brunger, and G. García, Phys. Rev. A **88**, 042702 (2013).
[8]W. Y. Baek, A. Arndt, M. U. Bug, H. Rabus, and M. Wang, Phys. Rev. A **88**, 032702 (2013).
[9]I. Nenner and G. J. Schulz, J. Chem. Phys. **62**, 1747 (1975).
[10]A. Modelli, P. Bolognesi, and L. Avaldi, J. Phys. Chem. A **115**, 10775 (2011).
[11]M. C. Fuss, L. Ellis-Gibbings, D. B. Jones, M. J. Brunger, F. Blanco, A. Muñoz, P. Limão-Vieira, and G. García, J. Appl. Phys. **117**, 214701 (2015).
[12]See supplementary material at http://dx.doi.org/10.1063/1.4937790 for data in numerical form.
[13]K. Regeta and M. Allan, Phys. Rev. A **91**, 012707 (2015).
[14]M. Allan, C. Winstead, and V. McKoy, Phys. Rev. A **77**, 042715 (2008).
[15]M. Allan, Phys. Rev. A **81**, 042706 (2010).
[16]F. H. Read and J. M. Channing, Rev. Sci. Instrum. **67**, 2373 (1996).
[17]M. Zubek, N. Gulley, G. C. King, and F. H. Read, J. Phys. B: At., Mol. Opt. Phys. **29**, L239 (1996).
[18]A. Gopalan, J. Bömmels, S. Götte, A. Landwehr, K. Franz, M. W. Ruf, H. Hotop, and K. Bartschat, Eur. Phys. J. D **22**, 17 (2003).
[19]J. C. Nickel, P. W. Zetner, G. Shen, and S. Trajmar, J. Phys. E: Sci. Instrum. **22**, 730 (1989).
[20]R. K. Nesbet, Phys. Rev. A **20**, 58 (1979).
[21]K. Takatsuka and V. McKoy, Phys. Rev. A **24**, 2473 (1981).
[22]K. Takatsuka and V. McKoy, Phys. Rev. A **30**, 1734 (1984).
[23]C. Winstead and V. McKoy, Adv. At., Mol., Opt. Phys. **36**, 183 (1996).
[24]C. Winstead and V. McKoy, Comput. Phys. Commun. **128**, 386 (2000).
[25]J. Tennyson, Phys. Rep. **491**, 29 (2010).
[26]P. G. Burke, *R-Matrix Theory of Atomic Collisions: Application to Atomic, Molecular and Optical Processes* (Springer, 2011).
[27]J. M. Carr, P. G. Galiatsatos, J. D. Gorfinkiel, A. G. Harvey, M. A. Lysaght, D. Madden, Z. Mašín, M. Plummer, J. Tennyson, and H. N. Varambhia, Eur. Phys. J. D **66**, 58 (2012).
[28]N. Sanna and F. A. Gianturco, Comput. Phys. Commun. **114**, 142 (1998).
[29]Z. Mašín and J. D. Gorfinkiel, J. Chem. Phys. **137**, 204312 (2012).
[30]W. Y. Baek, M. U. Bug, and H. Rabus, Phys. Rev. A **89**, 062716 (2014).
[31]G. L. Blackman, R. D. Brown, and F. R. Burden, J. Mol. Spectrosc. **35**, 444 (1970).
[32]J. Franz and F. A. Gianturco, Phys. Rev. A **88**, 042711 (2013).
[33]Y. Okamoto, K. Onda, and Y. Itikawa, J. Phys. B: At., Mol. Opt. Phys. **26**, 745 (1993).
[34]D. M. Chase, Phys. Rev. **104**, 838 (1956).
[35]Y. Itikawa, J. Phys. B: At., Mol. Opt. Phys. **37**, R1 (2004).
[36]N. F. Lane, Rev. Mod. Phys. **52**, 29 (1980).
[37]Z. Mašín, "Resonance formation in electron collisions with pyrimidine-like targets," Ph.D. thesis, The Open University, Milton Keynes, UK, 2012.
[38]K. Regeta, M. Allan, Z. Mašín, and J. D. Gorfinkiel, J. Chem. Phys. **144**, 024302 (2016).